

Multi-cycle Growth of Boron Doped ZnO Films as Photoanode for Dye-Sensitized Solar Cell (DSSC)

L. Roza, M.Y.A. Rahman*, A.A. Umar*, M.M. Salleh

Institute of Microengineering and Nanoelectronics (IMEN), Universiti Kebangsaan Malaysia (UKM), Bangi, 43600, Selangor, Malaysia

*E-mail: mohd.yusri@ukm.edu.my, akrajas@ukm.edu.my

Received: 1 July 2016 / Accepted: 2 September 2016 / Published: 10 November 2016

The work is concerned with the fabrication of dye sensitized solar cell (DSSC) utilizing multi-layer boron doped ZnO nanorods films. The B-doped ZnO films were prepared on FTO glass substrate via seed mediated hydrothermal method. Multi-layer B-doped ZnO nanorods were obtained by immersing the sample into a growth solution and repeated the growth process at 90 °C for 30 minutes. The structure of the B-doped ZnO film has been found to exhibit the hexagonal wurtzite structure. The length and diameter of the nanorods increase with the number of the growth cycle. The performance of the DSSC fabricated using the multi-layer B-doped ZnO nanorod was found to be significantly higher than that of the DSSC based on the single layer ZnO nanorod arrays. The best photovoltaic parameters with the J_{SC} of 3.5 mA cm⁻², FF of 0.38 and η of 0.67%, respectively was obtained for the device utilizing the layer with 3 cycles since it possesses the lowest photoluminescence in visible region and lowest R_{ct} .

Keywords: ZnO, boron, dye-sensitized solar cell, hydrothermal, nanorod

1. INTRODUCTION

Zinc oxide (ZnO) is material that has n-type semiconductor properties [1]. This material has several potential advantages as the most promising alternative over TiO₂ for working electrode application in DSSC due to inexpensive, high stability and ease of crystallization and anisotropic growth with scalable processing methods. Moreover, ZnO has higher electron mobility than that of TiO₂ which may reduce electron recombination with hole in DSSC. Wurtzite phase of ZnO is a common phase for the photoanode of DSSC. The ability to tune the properties of this oxide to suit the photovoltaic application and hence optimizing the performance of the device is a big challenge. Doping of ZnO offers an opportunity to achieve this in a cost-effective manner. Doping of ZnO with

metal such as tin, indium and boron yielded the efficiency of the DSSC of 1.82, 0.56 and 1.56%, respectively [2-4].

Various techniques have been used to prepare ZnO films nanostructure such as thermal evaporation [5], pulsed laser deposition (PLD) [6], magnetron sputtering [7], metal-organic chemical vapor deposition (MOCVD) [8] and chemical vapor deposition [9]. These techniques are able to synthesize ZnO nanostructures with various morphologies such as nanowires, nanorods, nanoflowers, nanobelts and nanoparticles. However, these techniques require expensive equipment and unsuitable for large scale sample preparation. Chemical solution technique in preparing ZnO nanostructure has several advantages over those growth techniques. Not only it is an inexpensive process which only requires low-cost equipment, but ZnO with excellent chemical and thermal stability can also be produced from this process. Multi-step growth process was reported to increase the properties of ZnO nanorods such as length and density [10]. Multi-step growth of ZnO nanorods on FTO substrate as a photoanode in DSSC prepared via hydrothermal method has been reported in [11]. A thicker film absorb more lights, but only the excitons created near the active interface are split into free electrons and holes and flows into an external circuit.

In our previous work, seed mediated hydrothermal technique at with the growth temperature of 90 °C and growth time of 8 h and followed by cooling down process to 50 °C for 16 h was employed to prepare ZnO nanotubes [1]. While, in this work, various growth cycles of seed mediated hydrothermal technique were used to modify the grain size, length and density of B-doped ZnO nanorods. Multi-step growth process was performed by changing growth solution with new growth solution and repeating the process with the same concentration and growth time duration. This technique was believed to extend the length of nanorods as a strategy to modify the surface morphology of the nanorods. The objective of the work is to investigate the influence of the properties of the B-doped ZnO on the performance parameters of the DSSC.

2. EXPERIMENTAL

The boron doped ZnO samples were grown on FTO substrate via seed mediated hydrothermal technique described in [12]. Reagent grade of boric acid with 99% purity (Sigma-Aldrich), $\text{Zn}(\text{NO}_3)_2 \cdot 6\text{H}_2\text{O}$ with 99% purity (Alfa Aesar) and HMT powders (99.0% in purity, Acros Organic) were used without any further purification. To grow the sample, the substrate coated with ZnO seed layers was subsequently immersed in a equimolar solution, containing 0.04 M of $\text{Zn}(\text{NO}_3)_2 \cdot 6\text{H}_2\text{O}$ and HMT. Then, 2 % wt. boric acid as boron source was added into the solution and the growth reaction was carried out at 90 °C for 8 h inside an oven. The solution was subsequently cooled down to 50 °C and the reaction was left for 16 h. After the growth process, the samples were then taken out of the solution, washed several times using pure water and dried using a flow of nitrogen gas. After the above stage, the growth process was then continued by re-immersing the sample into fresh growth solution and followed the growth process at 90 °C for 30 minutes. These processes were repeated for the next sample by renewing the growth solution from two to four times for every 30 minutes at 90 °C to produce B doped ZnO sample with various thicknesses. First, second, third and fourth growth cycle are

indicated as 1x, 2x, 3x and 4x, respectively. The samples were then dried using a flow of nitrogen gas for characterizations.

The morphology of the B-doped ZnO samples was characterized by using field emission scanning electron microscopy (FESEM, Carl Zeiss-Sigma). The outer diameter of the ZnO nanorods was estimated by using the scale located at the lower corner of the FESEM images. The thickness of the nanotubes was estimated from the cross-sectional image of the FESEM. The elemental composition of the samples was identified by Energy-dispersive X-ray spectroscopy (EDX) at the electron acceleration energy of 8 keV. The structure of the samples was examined by x-ray diffraction (XRD) model Bruker D8 Advance. The source of x-ray was Cu-K α with the wavelength of 1.5406 Å. The diffraction angle (2θ) was set in the range 20-60° with the scanning speed of 0.020 °s⁻¹. The optical properties of the ZnO samples were investigated using UV-Vis absorption and photoluminescence (PL) measurements. The PL measurement was performed at room temperature. Photoluminescence spectrophotometer model Edinburgh Photonic FLS 920 was employed to study the photoluminescence of the samples. A 450 W xenon light was used as light source with the excitation wavelength of 310 nm. Optical spectrophotometer UV-Vis Lambda 900 Perkin Elmer was employed to study the optical absorption of the samples.

2.3 Fabrication and performance study of DSSC

All samples were immersed into an ethanolic solution of 0.3 mM N719 dye for 2 h. The dipping time above 2 hours will etch the B-doped ZnO films on the substrate. The samples were then taken out, rinsed gently with fresh ethanol and then dried under a flow of nitrogen gas. Platinum film as a counter electrode was prepared by spin coating plastisol solution on the ITO substrate. An electrolyte containing 0.5 M LiI/0.05 M I₂/0.5 M TBP in acetonitrile was used as a redox couple. A DSSC was fabricated by sandwiching the parafilm between the B-doped ZnO photoanode and platinum counter electrode. The electrolyte was injected into a space between the photoanode and counter electrode and filled via a capillary. The performance study of the cell was carried out by observing the current-voltage behavior in the dark and under illumination using an AM 1.5 simulated light with an intensity of 100 mW cm⁻². The illuminated area of the cell was 0.23 cm². The current-voltage curves in the dark and under illumination were recorded by a Keithley high-voltage source model 237 interfaced with a personal computer. Six devices were fabricated utilizing the B-doped ZnO sample with the same number of growth cycle in order to calculate the standard deviation of photovoltaic parameters.

The electrochemical impedance spectroscopy (EIS) model Vertex was performed at room temperature in dark to determine the bulk resistance (R_b) and charge transfer resistance (R_{ct}) of the devices. The devices were applied to the forward bias voltage at 0.5 V. The scanning frequency used was in the range 0.1 Hz-1 MHz with the perturbation voltage of 30 mV.

3. RESULTS AND DISCUSSION

Fig. 1 depicts the top view FESEM images of the B-doped ZnO samples grown via multi-cycles growth. From the figure, it is obviously noticed that the morphological shape of the samples is nanorod. The nanorods are not parallel to each other and not compact since there are a lot of pores found between the nanorods. The samples are inhomogeneous since the nanorods size are not identical. The nanorod diameter illustrated in Table 1 was found to increase with the number of growth cycle. This is due to the growth process was continued by adding new source of Zn^{+2} and OH^- , assuming that the ions of the precursor consumed and the growth process was complete in the growth solution. Through the immersion of the sample into the next growth solution, the growth process could be continued. The next growth solution reproduce newly ion precursor such as Zn^{+2} and OH^- source to initiate the nucleation process, then produces longer nanorods.

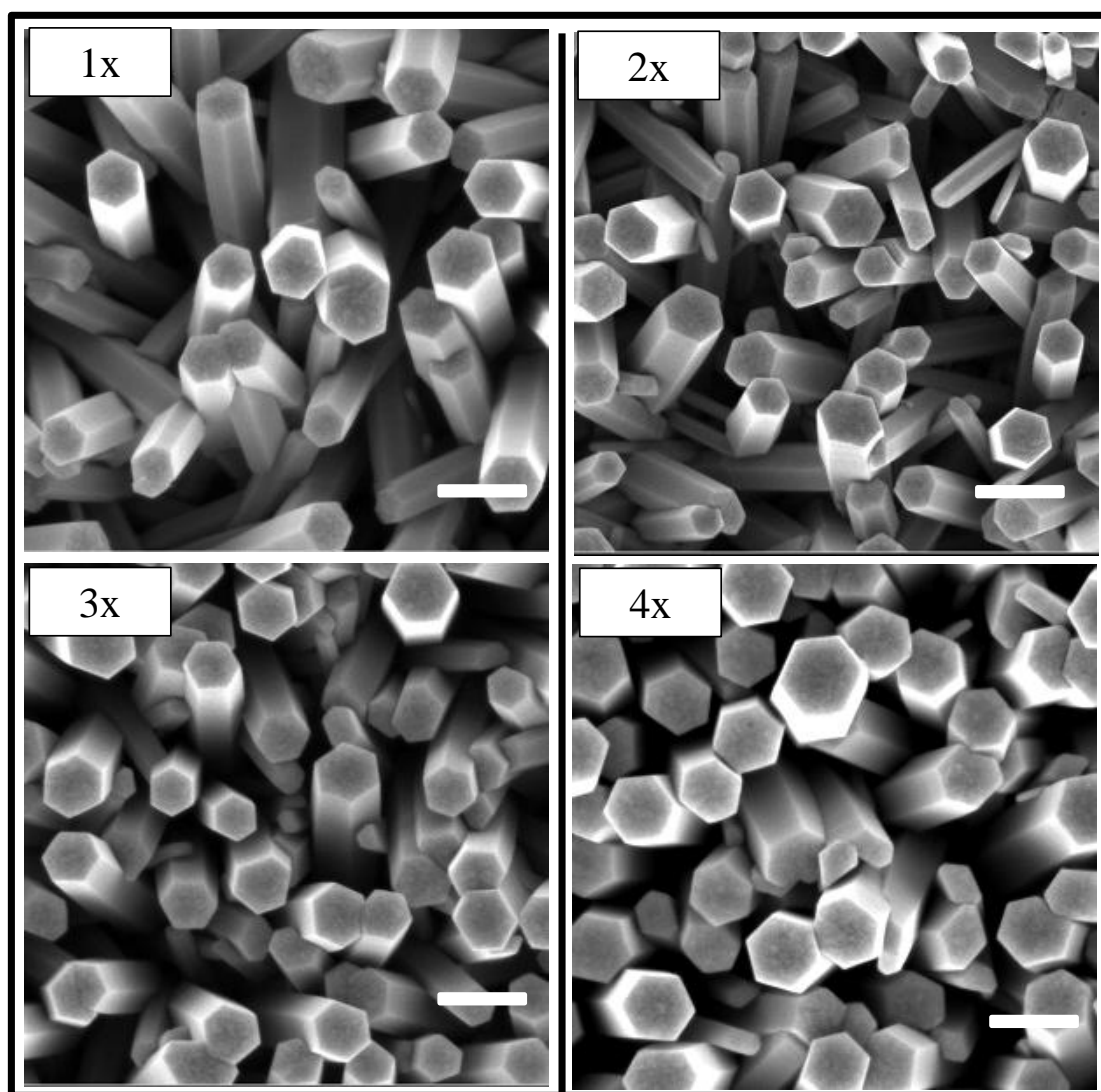


Figure 1. FESEM images of B-doped ZnO sample grown via multi-cycles growth process, scale bar 200 nm

Fig. 2 shows the FESEM cross-sectional images of the samples grown via multi-cycles growth. From Fig. 2, it is found that the growth direction of the nanorods becomes slanted once the number of growth cycle is increased. The nanorod length was found to increase with the number of growth cycle. The nanorod length is illustrated in Table 1.

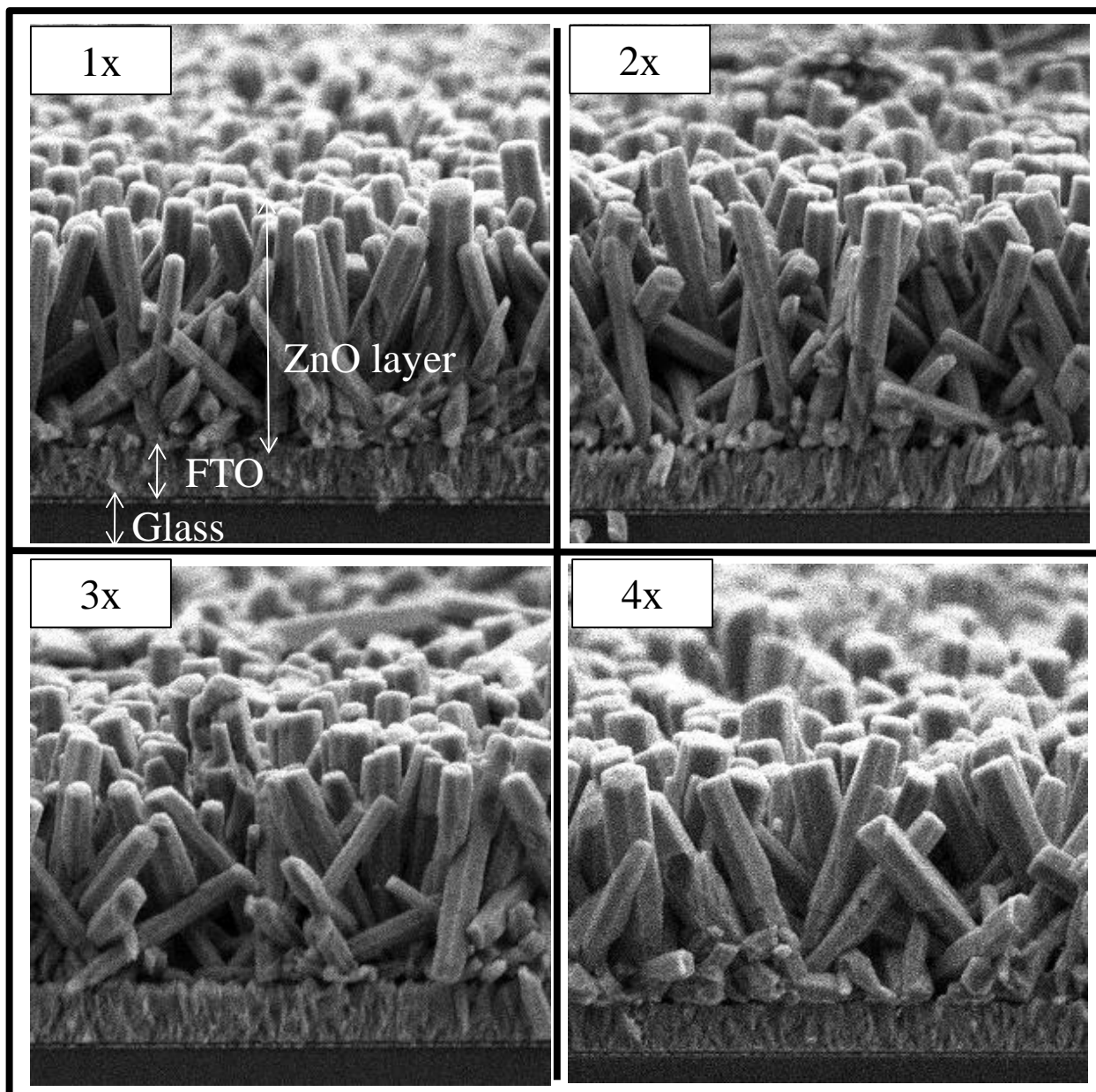


Figure 2. FESEM cross-sectional images of B-doped ZnO nanorods sample grown via multi-cycles growth process

Fig. 3 illustrates the EDX spectra for all samples grown via multi-cycles of growth. The spectra show the peaks of Zn and O elements, indicating the presence of these elements in the samples. However, the peak of B is not found in the spectra since its weight and atomic percentage are much smaller than those of Zn and O as illustrated in each elemental composition table in the spectra. The

small weight and atomic percentage of boron is due to small weight percentage of boron source that is 2 % wt. boric acid. The peak of C is also not found in the spectra as its weight and atomic percentage are small, similar to those of B. The Zn weight and atomic percentage gradually decreases but those of boron increases as the number of growth cycle increases, signifying an increment in the sample thickness. This phenomenon is normal since if the weight and atomic percentage of a particular element increases, those of another element decrease.

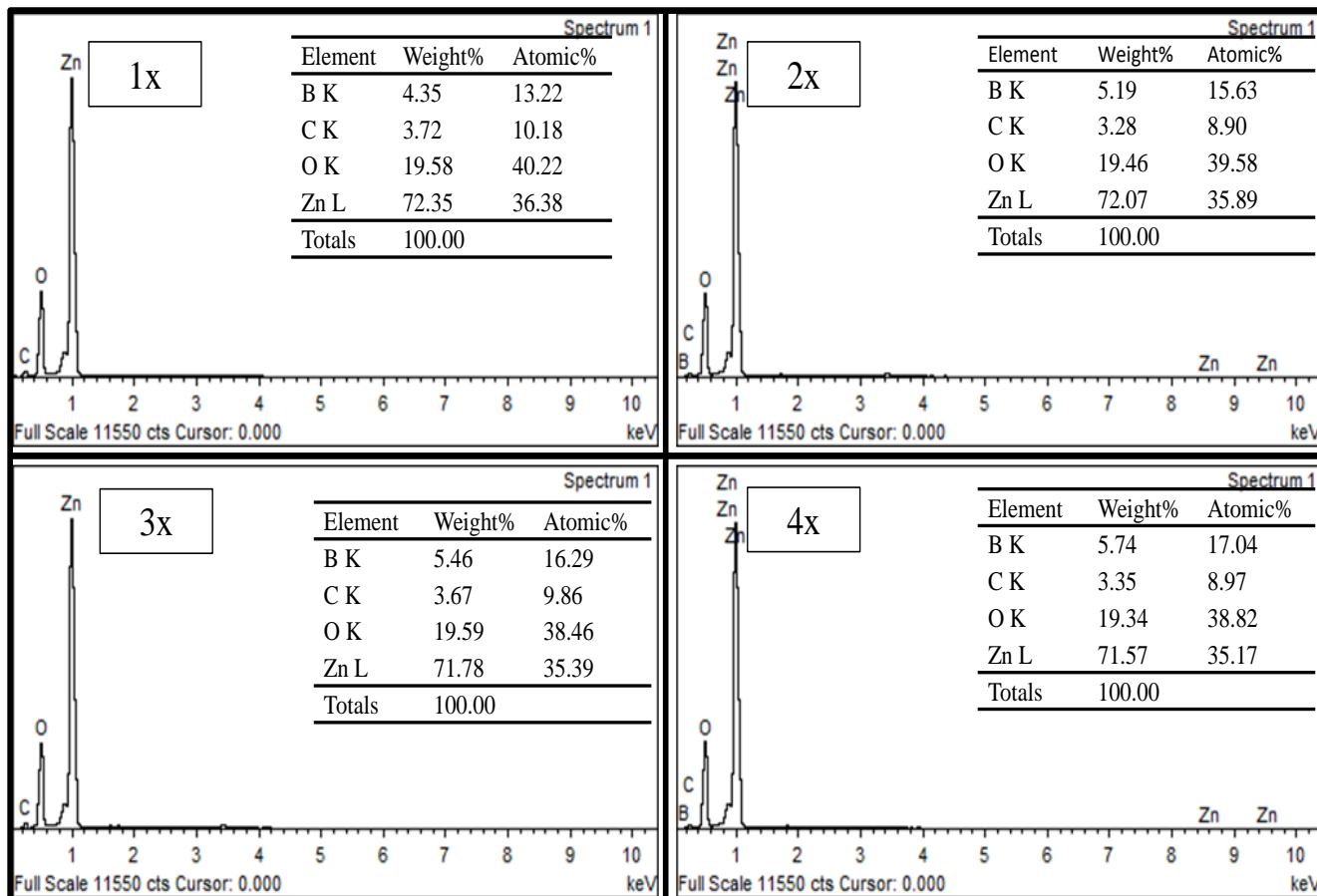


Figure 3. EDX spectra of B-doped ZnO nanorods sample grown via multi-cycles growth process

Fig. 4 shows the XRD patterns of B-doped ZnO samples prepared via various growth cycles. It indicates that most of the crystals in the samples have a strong orientation along the *c*-axis (002) plane as reported in JCPDS card (file no.36-1451). The diffraction patterns show three wurtzite phase peaks at 33.90°, 36.39°, and 47.48°, respectively [12]. According to the JCPDS card, the peaks are attributed to (002), (101) and (102) plane, respectively. The crystal structure is hexagonal. The height of peak intensity of the (002) peak is about the same. The full width half-maxima (FWHM) of the peaks are also about the same, signifying that the crystallite size of the sample is about the same according to the Scherrer formula.

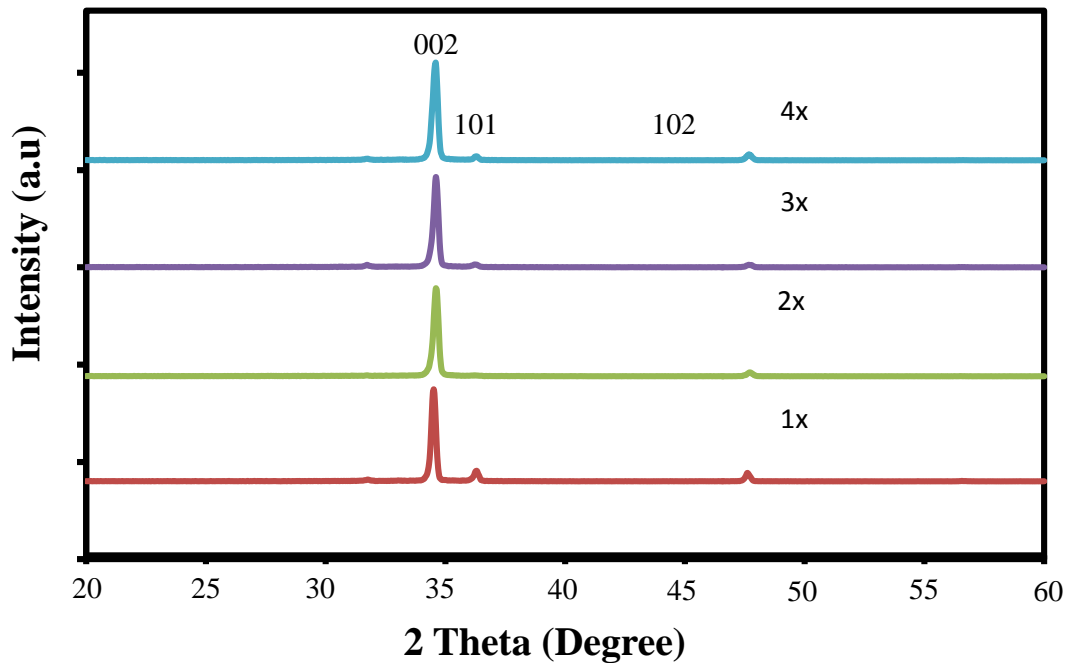


Figure 4. XRD spectra of B-doped ZnO nanorods sample grown via multi-cycles growth process

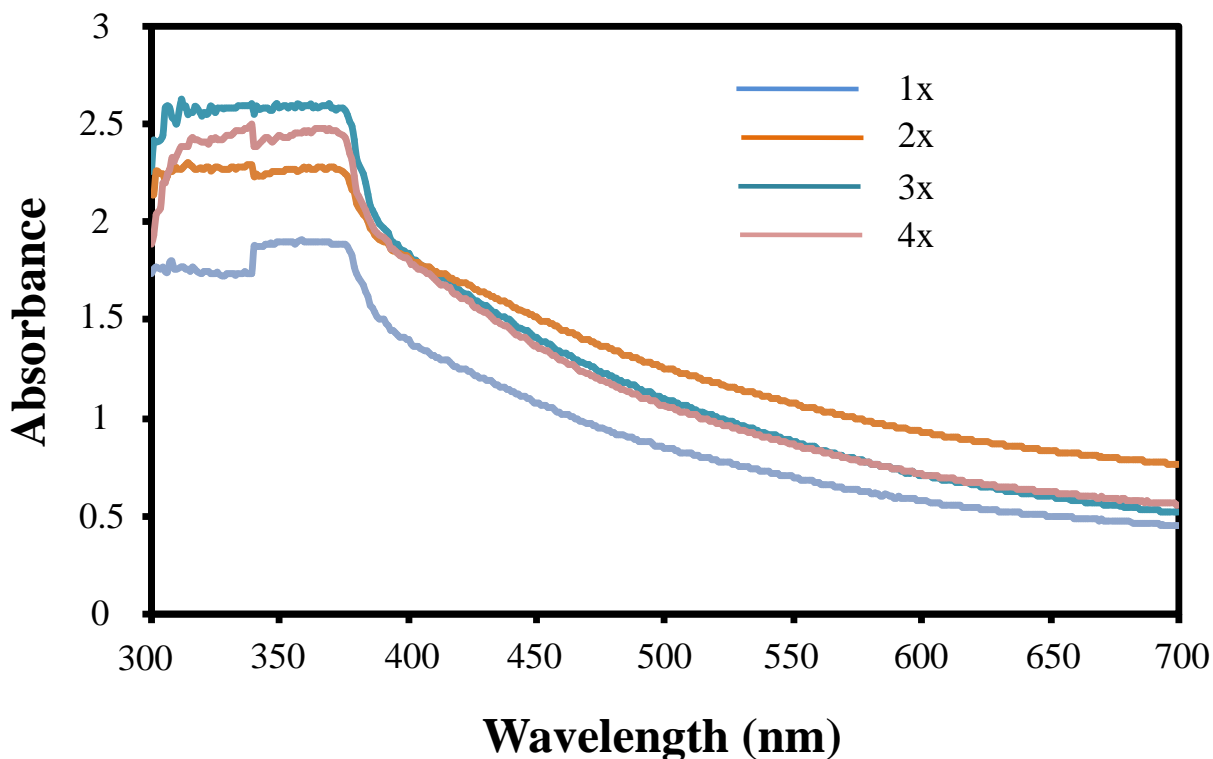


Figure 5. UV-VIS optical absorption spectra of B-doped ZnO nanorods sample grown via multi-cycles growth process

Fig. 5 presents the optical absorption spectra of the samples grown via multi-cycles growth. The UV-Vis spectra show quite similar pattern in the range of 300-700 nm. The spectra show strong

absorption at the wavelength of 380 nm and weak absorption after 380 nm in the range from visible to near infrared. The spectra also show the absorption saturation at 380 nm for all samples. The spectra are typical for the non-coated dye samples in which the samples absorb more light in UV region rather than visible region. It is obvious that the absorption of the sample increases as the number of growth cycles increases. The absorption for the sample prepared with 3th cycle growth possesses the highest absorption spectra in UV light range, while the lowest absorption belongs to the single growth cycle sample due to it has the smallest diameter of the nanorods. The sample with the highest peak indicates that the sample absorb more light within UV region.

Fig. 6 presents the room temperature PL spectra of the samples grown via multi-cycles growth. All spectra show identical characteristic, where two main emissions band were present. The recombination process was created from emission band in visible region at 370 nm. The sample with 2nd cycle growth process possesses the highest photoluminescence peak, followed by 1st, 3 and 4th cycle sample at 390 and 440 nm. These results indicate that the 2nd cycle sample has the highest rate of recombination between electron and hole, followed by 1st, 3 and 4th cycles samples. A broad and intense green emission band is well known as deep level emissions at approximately at 621 nm is related to structural defect in ZnO due to oxygen vacancies. The sample with 1st growth cycle possesses the most intense visible band which signifies the presence of structural defect in the sample. On other hand, the sample with 3rd growth cycle exhibits the lowest rate of recombination of electron-hole due to the less intense green-yellow emission indicating that lower defect was detected. The PL spectra patterns shown in this figure are quite similar to those reported in [13]. Commonly, defects in ZnO are either contributed by oxygen vacancy or formation of interstitial Zn [14].

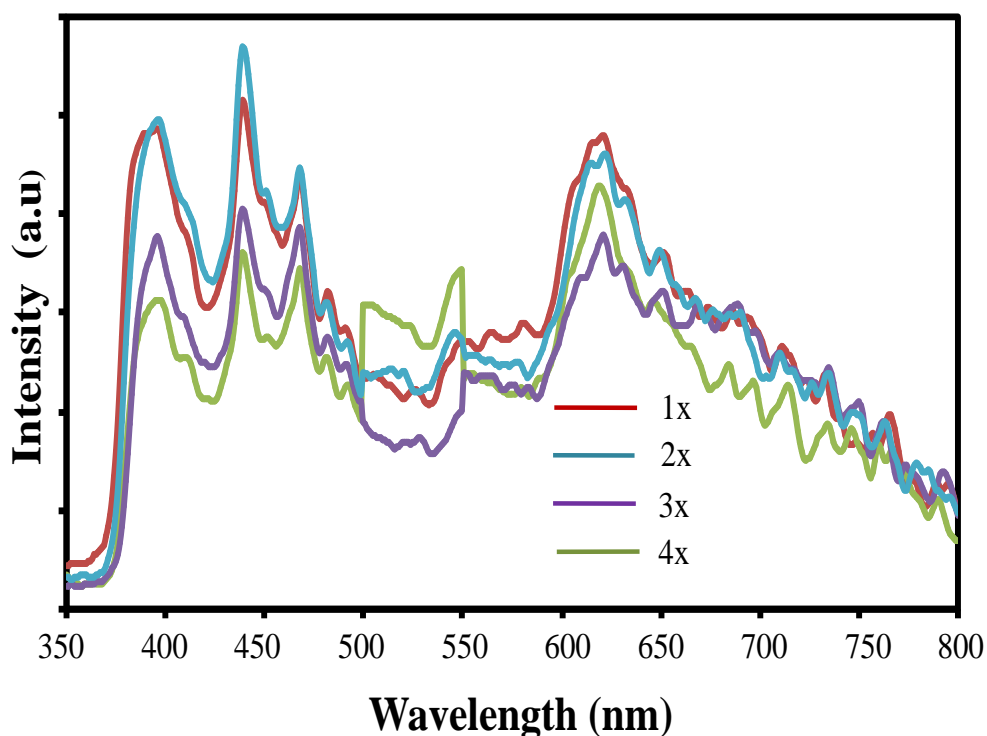


Figure 6. Photoluminescence spectra of B-doped ZnO nanorods sample grown via multi-cycles growth process

Fig. 7 shows the *I-V* curves of the DSSC utilizing B-doped ZnO sample synthesized at various number of growth cycles in dark. It is noticed from the figure that the devices do not show rectification property since the dark current in the reverse bias is slightly higher than that in the forward bias. The current in reverse bias is also called leak current. The higher leak current, the smaller photocurrent and consequently the smaller output power generated in the device as shown in Fig. 8. However, the device allows quite high dark current in both biases which is in the mA range. For both biases, the different in the current for all devices is small indicating that the number of growth cycle does not affect the dark current.

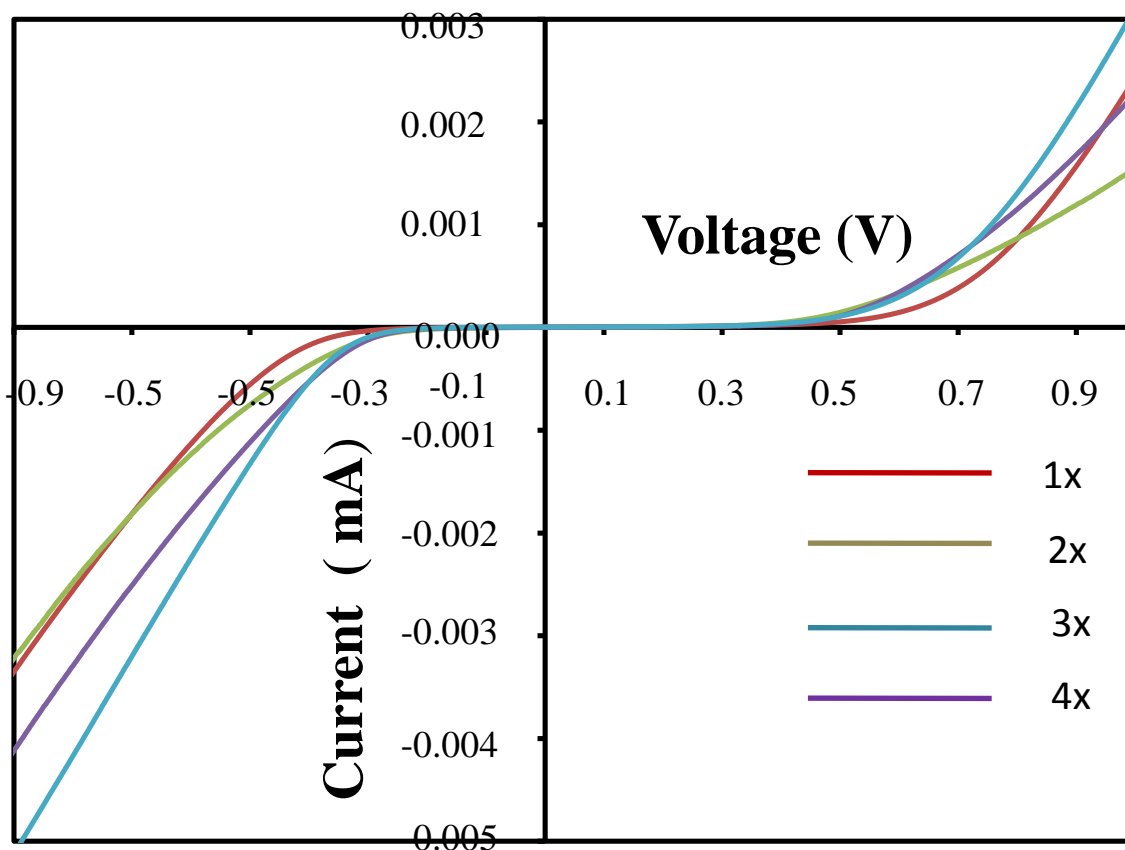


Figure 7. Dark current of the DSSC utilizing B-doped ZnO nanorods sample grown via multi-cycles growth process

Fig. 8 shows the *J-V* curves of the devices utilizing the samples grown via multi cycles of growth process under 100 mW cm^{-2} light illuminations at room temperature. The DSSC utilizing the samples with 1st, 2nd and 3rd growth cycles perform the increasing trend of the output power and decreases at the DSSC sample prepared with 4th growth cycle. The slope of each curve is quite high, indication of high internal resistance of the devices, leading to high power loss and small fill factor (*FF*). The high power loss is related to high leakage current as illustrated in Fig. 9. The other photovoltaic parameters are presented in Table 1. According to Table 1, it was found that the DSSC utilizing ZnO nanorods with 3rd growth cycle demonstrates the optimum J_{SC} and η . This is due to this

device possesses the lowest photoluminescence in visible region as illustrated Fig. 6. The highest η of 0.67% is higher than those obtained from our previous work [12] which was 0.29% corresponding with the B-doped ZnO layer thickness of 0.48 μm . However, the thickness of the B-doped ZnO sample of this work is 1.55 μm . The thicker sample provides the higher number of charge carrier be generated upon the light illumination on the device. The highest η of this work is also higher than those reported in [10,11,15], yielding 0.30%, 0.32% and 0.12% for the DSSC utilizing undoped ZnO photoanode. However, the highest η of this work is smaller than that reported in [4], demonstrating 1.56% of B-doped ZnO DSSC.

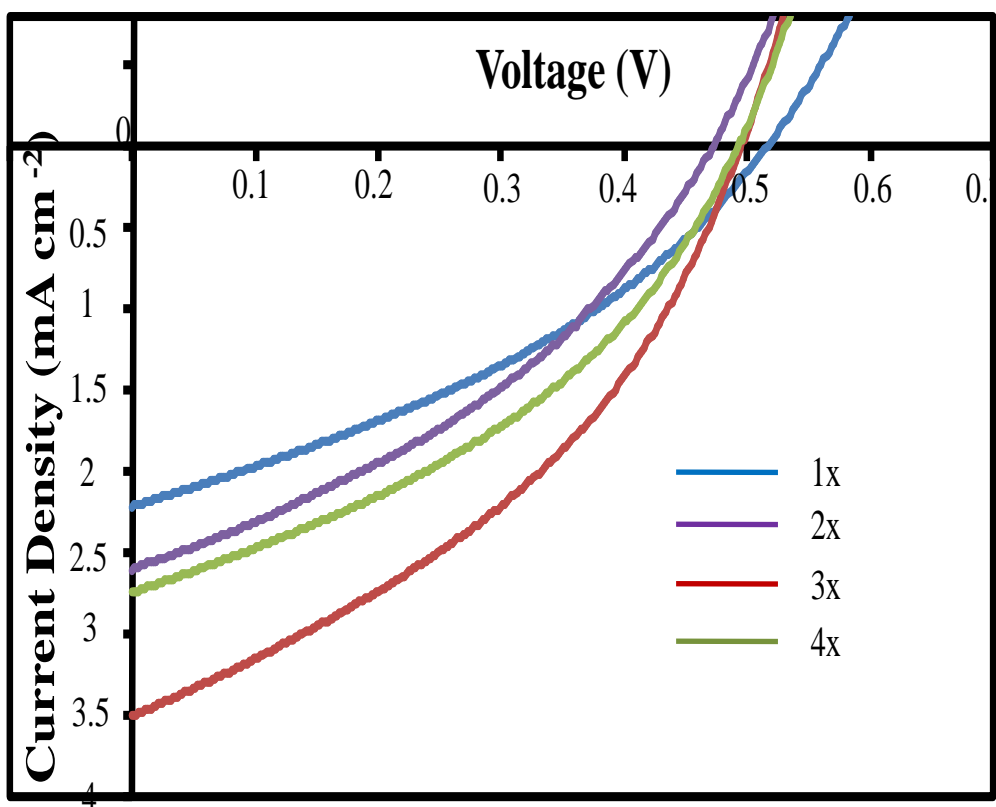


Figure 8. *J-V* curves of the devices utilizing the B-doped ZnO nanorods sample grown via multi-cycles growth process under 100 mW cm^{-2} light illuminations

Fig. 9 shows the nyquist plots of the DSSC utilizing the samples grown at various growth cycles. There are three arcs shown in the plots but the third arc representing the charge transfer resistance at electrolyte/platinum interface is not discussed since it is incomplete semicircle. The 2nd growth cycle sample does not show third arc. The plots show two overlapped semicircles representing the bulk resistance (R_b) and charge transfer resistance (R_{ct}). The smaller semicircle represents R_b and the bigger one represents R_{ct} . The bulk resistance of the device is contributed by FTO, B-doped ZnO film, N719 dye, electrolyte containing Γ^-/I_3^- and platinum counter electrode. While, the charge-transfer resistance is attributed to the impedance based on charge-transfer processes occurring at B-doped ZnO/dye/redox (Γ^-/I_3^-)[16]. These EIS data are presented in Table 1. The DSSC utilizing the sample

grown at 3rd cycle demonstrates the lowest R_b , followed by 2nd, 4th and 1st samples. The DSSC utilizing the sample grown at 3rd cycle demonstrates the lowest R_{ct} , followed by 4th, 2nd, 7th and 1st samples. It is noticeable that the R_{ct} data are consistent with the photovoltaic parameters of J_{sc} and η . The lower R_{ct} , the higher J_{sc} and η . Fig. 10 shows the equivalent circuit representing the nyquist plot in which R_{ct} contributed by the charge-transfer resistance at B-doped ZnO/N719/electrolyte is parallel with constant phase element 1 (CPE1). CPE2 is parallel with R_{ct} which is contributed by the charge-transfer resistance at electrolyte/platinum which is not counted in this work. Both CPE1 and CPE2 are imaginary resistances.

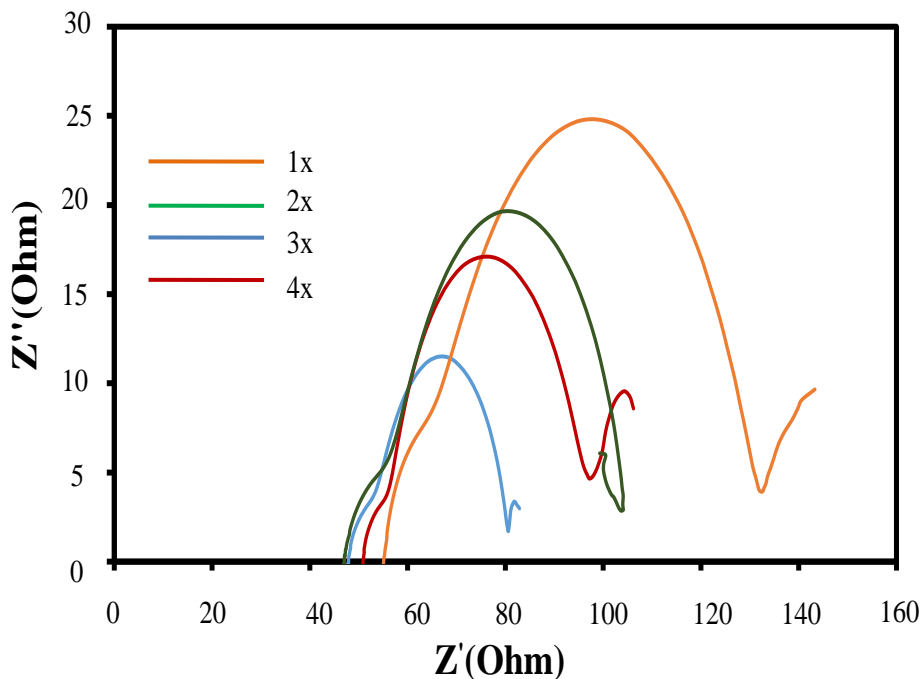


Figure 9. Nyquist plots of the DSSC utilizing the B-doped ZnO sample grown via multi-cycles growth process

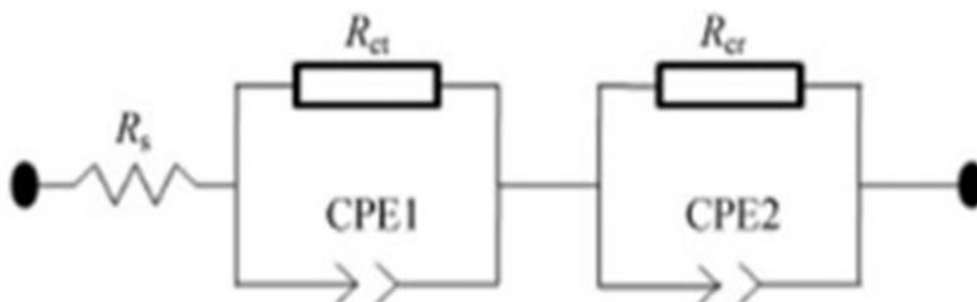


Figure 10. Equivalent circuit corresponding with the Nyquist plot

Table 1. Length, diameter, photovoltaic parameters and EIS data for the DSSC utilizing B-doped ZnO grown via multi-cycles growth process

| Growth cycle | Length (μm) | diameter (nm) | V_{OC} (V) | J_{SC} (mA cm^{-2}) | FF | η (%) | R_b (Ω) | R_{ct} (Ω) |
|--------------|--------------------------|---------------|-----------------|----------------------------------|-----------------|-----------------|--------------------|-----------------------|
| 1 | 1.36 \pm 10 | 185 \pm 12 | 0.48 \pm 0.03 | 2.23 \pm 0.05 | 0.36 \pm 0.03 | 0.41 \pm 0.03 | 13 \pm 1 | 65 \pm 2 |
| 2 | 1.42 \pm 10 | 236 \pm 12 | 0.50 \pm 0.03 | 2.65 \pm 0.06 | 0.36 \pm 0.03 | 0.45 \pm 0.03 | 6 \pm 1 | 50 \pm 2 |
| 3 | 1.55 \pm 20 | 262 \pm 10 | 0.50 \pm 0.03 | 3.51 \pm 0.03 | 0.38 \pm 0.03 | 0.67 \pm 0.03 | 5 \pm 1 | 27 \pm 2 |
| 4 | 1.65 \pm 10 | 289 \pm 10 | 0.50 \pm 0.03 | 2.86 \pm 0.05 | 0.38 \pm 0.03 | 0.52 \pm 0.03 | 11 \pm 1 | 47 \pm 2 |

4. CONCLUSIONS

The effect of the number of growth cycles on the properties of B-doped ZnO nanorods film and the performance of the DSSC has been investigated. The length and diameter of nanorods increase with the increase in the number of growth cycle. The results of absorption spectra and photoluminescence (PL) analysis indicate that strong absorption and reduced recombination of electron-hole have been achieved with the sample produced after treatment with 3rd cycle. The best photovoltaic parameters with the J_{SC} of 3.50 mA cm^{-2} and η of 0.67%, respectively was obtained from the device utilizing the layer with 3 cycles due the lowest photoluminescence in visible region and lowest R_{ct} . The J_{sc} and η increase with the decrease in R_{ct} .

ACKNOWLEDGMENTS

This work was supported by the Ministry of higher Education of Malaysia under research grant FRGS/2/2013/SG02/UKM/02/5 and DLP-2015-003. This work was also supported by the Ministry of Research, Technology and Higher Education of Indonesia under research grant KLN (International Research Collaboration and Scientific Publication 2015) contract no. 550/UN.19.1/LPPM/2015.

References

1. L. Roza, M.Y.A. Rahman, A.A. Umar, M.M. Salleh, *J. Alloys Compd.* 618 (2015) 153-158.
2. S. Ameen, M.S. Akhtar, H.K. Seo, Y.S. Kim, H.S. Shin, *Chem. Eng. J* 187 (2012) 351-356.
3. A. Tubtintae, M.W. Lee, *Superlatt. Microstruc.* 52 (2012) 987-996.
4. V. Kumar, N. Singh, V. Kumar, L.P. Purohit, A. Kapoor, O.M. Ntwaeaborwa, H.C. Swart, *J. Appl. Phys.* 114 (2013) 134506.
5. N. Bouhssira, S. Abed, E. Tomasella, J. Cellier, A. Mosbah, M.S. Aida, M. Jacquet, *Appl. Surf. Sci.* 252 (2006) 5594-5597.
6. B.J. Jin, S.H. Bae, S.Y. Lee, S. Im, *Mater. Sci. Eng. B* 71 (2000) 301-305.
7. C. Wang, Z. Chen, Y. He, L. Li, D. Zhang, *Appl. Surf. Sci.* 255 (2009) 6881-6887.
8. E. Galoppini, J. Rochford, H. Chen, G. Saraf, Y. Lu, A. Hagfeldt, G. Boschloo, *J. Phys. Chem. B* 110 (2006) 16159-16161.
9. M. Purica, E. Budianu, E. Rusu, M. Danila, R. Gavrilă, *Thin Solid Films* 403-404 (2002) 485-488.
10. J.B. Baxter, A.M. Walker, K. vanOmmering, E.S. Aydil, *Nanotechnology* 17 (2006) S304- S312.
11. H. Gao, G. Fang, M. Wang, N. Liu, L. Yuan, C. Li, L. Ai, J. Zhang, C. Zhou, S. Wu, X. Zhao, *Mater. Res. Bull.* 43 (2008) 3345-3351.
12. M.Y.A. Rahman, L. Roza, A.A. Umar, M.M. Salleh, *J. Alloys Compd.* 648 (2015) 86-91.

13. D. Li, Y.H. Leung, A.B. Djurišić, Z.T. Liu, M.H. Xie, S.L. Shi, S.J. Xu, *Appl. Phys. Lett.* 85 (2004) 1601-1603.
14. A B. Djurišić, Y.H. Leung, *Small* 2 (2006) 944-961.
15. S. Suresh, A. Pandikumar, S. Murugesan, R. Ramaraj, Samuel Paul Raj, *Solar Energy* 85 (2011) 1787-1793.
16. S.-C. Yang, D.-J. Yang, J. Kim, J.-M. Hong, H.-G. Kim, I-D. Kim, H. Lee, *Adv. Mater.* 20 (2008) 1059-1064.

© 2016 The Authors. Published by ESG (www.electrochemsci.org). This article is an open access article distributed under the terms and conditions of the Creative Commons Attribution license (<http://creativecommons.org/licenses/by/4.0/>).